JOURNAL OF MATERIALS SCIENCE 30 (1995) 1018–1024

Low-velocity impact damage in brittle coatings

CHIN-CHEN CHIU, YUNG LIOU
Institute of Physics, Academia Sinica, Taipei, Taiwan, Republic of China

Based on thin plate/elastic foundation theory and strain energy release rate calculations, this paper presents a lateral crack model to analyse the threshold for and development of impact damage in brittle coatings. Numerical solutions indicate that an increase in coating-to-substrate elastic modulus ratio tends to enhance the coating's resistance to impact damage initiation. The size of the lateral crack in a coating layer is a function of the coating thickness. For comparison with the theoretical prediction, experiments were performed on SiC-coated graphite specimens, as well as on glass microscope slides resting on various kinds of substrates.

1. Introduction

Ceramic coatings, for example TiN coatings on steels [1], can behave as protective layers for substrates against erosive wear. In such applications, the coatings may be cracked as a result of impact. Thus, there is a need to understand fully the impact damage development for coating design and material selection.

It is generally accepted [1–14] that the resistance of a coated surface to impact damage is associated with the following parameters: (1) coating-to-substrate elastic modulus ratio; (2) the pre-existing microcracks and residual stress in the coating; and (3) coating thickness, toughness, hardness, and microstructure. For example, Liaw *et al.* [7] proposed an elasto-dynamic finite element model to replicate impact damage experiments on monolithic zirconia and then to predict further impact damage in zirconia-coated steels. They reported [7] that coating thickness affected the pattern of damage in the zirconia coating. Some researchers [8–11] have used classical elasticity theory to analyse the quasi-static contact stress field in coated materials, and have shown that the stress field is a function of coating-to-substrate elastic modulus ratio. Based on dynamic stress wave propagation, Springer [12] showed that water droplet-induced failure was related to the material properties of the coating and substrate.

Coated materials can be considered as an elastic plate of finite thickness but infinite extent bonded to a semi-infinite elastic foundation. Such plate-foundation interaction problems have been analysed widely for the design of structural foundations, such as pavement systems [13]. In the present paper, the threshold for and development of impact damage in a coating is studied qualitatively by using a combination of thin plate/elastic foundation theory [13, 14] and strain energy release rate calculations to obtain numerical solutions. The theoretical prediction is compared with experimental results on SiC-coated graphite specimens and model layered specimens.

2. Theoretical considerations

2.1. Strain energy analysis

Fig. 1 illustrates an impactor of mass M and velocity V striking a semi-infinite solid coated with a surface layer. From the viewpoint of quasi-static stress analysis, a low-velocity impact on a coated solid can be approximated as the problem of contact against infinite elastic plate bonded to a semi-infinite homogeneous elastic foundation [8, 15, 16]. The contact area is assumed to be small enough so that the impact loading can be regarded as a point load [15]. The corresponding static load is calculated from the kinetic energy of the impactor by the principle of conservation of total energy of the impactor by the principle of conservation of total energy [16]. Thus, the strain energy in the coating can be evaluated from thin plate/elastic foundation theory [13, 17].

When a concentrated load, P, acts on a coated solid, the axisymmetric flexure of the coating, $W(r)$, can be described by a nonhomogeneous biharmonic equation in terms of a cylindrical coordinate system (r, θ, z) with the origin at the loading point. The equation is

$$D\nabla^2\nabla^2 W(r) = P - Q(r) \tag{1}$$

where

$$D = \frac{E_c t_c^3}{12(1 - v_c^2)} \tag{2}$$

D is the flexural rigidity of the coating layer. ∇^2 and $Q(r)$ are the Laplacian operator and the contact stress at the coating/substrate interface, respectively. The subscripts, c and s, refer to properties of the coating and the substrate, respectively. E, t, and v are Young's modulus, thickness, and Poisson's ratio,

0022–2461

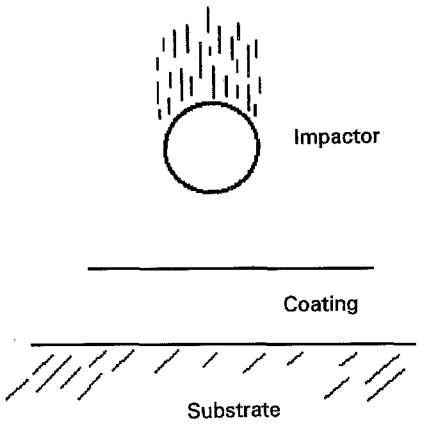

Figure 1 A schematic diagram of a particle impacting on a coated solid.

respectively. Selvadurai [13] and Sneddon *et al.* [14] solved Equation 1 and gave the following solutions

$$W(r) = \frac{P(1-v_s^2)}{\pi A E_s}\int_0^\infty \frac{J_0(xr/A)}{(1+x^3)}\,dx \tag{3}$$

$$Q(r) = \frac{P}{2\pi A^2}\int_0^\infty \frac{xJ_0(xr/A)}{(1+x^3)}\,dx \tag{4}$$

$$W(0) = 0.3849\,\frac{P(1-v_s^2)}{AE_s} \tag{5}$$

where

$$A = \left[\frac{2D(1-v_s^2)}{E_s}\right]^{\frac{1}{3}} \tag{6}$$

J_0 represents the zeroth order Bessel function of the first kind. $W(0)$ is the deflection of the coating at the point of loading. Equations 3, 4, and 5 are solutions corresponding to quasi-static loading conditions. To model low-velocity impact damage based on quasi-static stress analysis, this paper assumes that the kinetic energy of the impactor can transfer totally to the target. The energy loss from material damping and surface friction as well as the dynamical effects of strain rate and adiabatic temperature are neglected. Equating the kinetic energy of the impactor to the strain energy of the coated solid gives

$$1/2MV^2 = 1/2PW(0) \tag{7}$$

The term on the right hand side of Equation 7 represents the work done by the concentrated load, P. Combining Equations 5 and 7 yields

$$P = \left(\frac{MV^2AE_s}{0.3849(1-v_s^2)}\right)^{\frac{1}{2}} \tag{8}$$

Equation 8 gives a solution for the quasi-static load evaluated from the kinetic energy of the impactor.

According to plate theory, the strain energy of the coating in a circular region ($r \le r_0$) is calculated by [17]

$$U(r_0) = \pi D\int_0^{r_0}\left[\left(\frac{\delta^2W}{\delta r^2}+\frac{\delta W}{r\,\delta r}\right)^2 - \frac{2(1-v_c)}{r}\,\frac{\delta W}{\delta r}\,\frac{\delta^2 W}{\delta r^2}\right] r\,dr \tag{9a}$$

For convenience, Equation (9a) is rewritten in terms of a simple form

$$U(r_0) = \pi D\int_0^{r_0}\Phi(r)\,dr \tag{9b}$$

Differentiating Equation 3 gives

$$\frac{\delta W}{\delta r} = -\frac{P(1-v_s^2)}{\pi A^2 E_s}\int_0^\infty \frac{xJ_1(xr/A)}{(1+x^3)}\,dx \tag{10}$$

$$\frac{\delta^2 W}{\delta r^2}+\frac{\delta W}{r\,\delta r} = -\frac{P}{2\pi D}\int_0^\infty \frac{x^2J_0(xr/A)}{(1+x^3)}\,dx \tag{11}$$

J_1 is the first order Bessel function of the first kind. Combining Equations 9a, 10, and 11 yields the strain energy density distribution, dU/dr, in the coating (Appendix A).

2.2. Impact damage

Impact against a brittle coating may cause lateral cracking, radial cracking, Hertzian cone cracking, or coating/substrate interface debonding beneath the contact point [1, 2]. Generally speaking, the appearance, dimensions, number, positions, and the stressed state of the impact-induced cracks are complicated so that a study of every growing crack is difficult. The present paper proposes a lateral crack model to study qualitatively the threshold for and the development of impact damage in coatings. It is assumed that: (1) the as-deposited coating layer contains penny-shaped cracks of radius $r = C_i$, which are distributed throughout the material; (2) the pre-existing crack immediately beneath the impact point can be forced to propagate, developing into a lateral crack in the coating layer [1, 2, 18]; (3) this crack growth results in the release of strain energy from the coating; (4) Griffith's failure criterion determines when crack propagation and crack arrest occur; (5) the effective radius of the damaged region is equal to the radius of the lateral crack.

Fig. 2a is a schematic drawing of a cross section of an impact-induced lateral crack, which has been observed experimentally by some researchers [2, 7, 19]. For instance, Fig. 2b illustrates a scanning electron micrograph of such lateral cracks in a SiC-coating on a graphite specimen (see next section). The cross-section of the lateral crack appears to be an exponential curve. The distance from the free surface to the lateral crack surface, h, can be approximated by the following empirical equation (Appendix B)

$$h(r) = t_c\left[1-\exp\left(-\frac{r}{2t_c}\right)\right] \tag{12}$$

If the damaged region of the coating is considered as the superposition of two separate layers (Fig. 2a), the formation of a lateral crack causes a decrease in the flexural rigidity of the coating. Thus, the effective rigidity, D_{eff}, of a small element in the damaged region becomes

$$D_{\text{eff}} = \frac{E_c h^3}{12(1-v_c^2)} + \frac{E_c(t_c-h)^3}{12(1-v_c^2)} \tag{13}$$

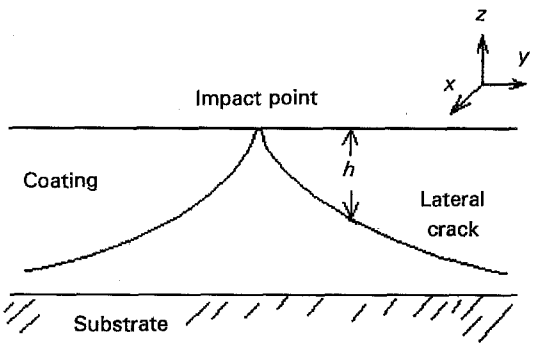

(a)

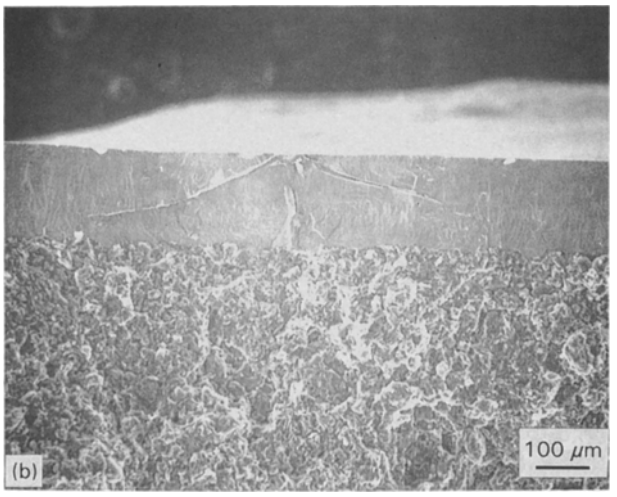

Figure 2 (a) A schematic diagram of the cross-section of an impact-induced lateral crack in the coating layer. (b) A scanning electron micrograph of the cross section of the lateral cracks in SiC coated graphite.

A substitution of Equation 12 into Equation 13 shows that D_{eff} is a function of the radius of the damaged region, r.

When the pre-existing crack beneath the impact point grows from $r = c_i$ to $r = c_f$, the flexural rigidity of coating and the strain energy decrease locally. To analyse the cracking effects further, it is assumed that impact damage does not change the flexure of the coating $W(r)$ before and after crack propagation. This means that the kinetic energy of the impactor is first converted into the strain energy stored in coated solid as the coating develops a certain flexural shape, $W(r)$. Then, crack growth occurs in the coating layer without further changing the shape of the coating (i.e. $W(r)$ is constant). Thus, impact damage decreases the effective rigidity and the strain energy in the damaged region ($r \leq c_f$). However, the impact damage does not affect the strain energy in the region ($r > c_f$), since the corresponding $W(r)$ and D do not change (see Equations 9, 10, and 11).

Because of the rigidity decrease from D to D_{eff}, the strain-released energy, L, by the damaged region of the coating ($r \leq c$) is given by

$$L(C) = \pi \int_0^C D_{\text{eff}}(r)\Phi(r)\mathrm{d}r - \pi D \int_0^C \Phi(r)\mathrm{d}r \quad (14)$$

The total area, B, of the lateral crack is the area obtained by rotating the exponential curve (Equation 12) around the z axis (see Fig. 2a). That is

$$B(C) = -2\pi \int_0^h \frac{2t_c \ln[(t_c - z)/t_c)]}{t_c - z} (5t_c^2 - 2t_c z + z^2)^{\frac{1}{2}} \mathrm{d}z \quad (15a)$$

$$= -2\pi \int_0^h \Omega(z)\mathrm{d}z \quad (15b)$$

where $\Omega(z)$ is defined by comparing Equation 15a with Equation 15b. Consequently, the strain energy release rate, G, is

$$G(C) = \frac{-\mathrm{d}L}{\mathrm{d}B} = \frac{-\mathrm{d}L/\mathrm{d}C}{\mathrm{d}B/\mathrm{d}C} = \frac{[D_{\text{eff}}(C) - D]\Phi(C)}{\Omega(h)\exp(-C/2t_c)} \quad (16)$$

where

$$h = t_c\left[1 - \exp\left(\frac{-C}{2t_c}\right)\right],$$

According to the Griffith criterion, the pre-existing cracks beneath the impact point will grow if $G > 2\tau$, where τ is the fracture surface energy of the coating material, and crack arrest will occur when $G < 2\tau$. Consequently, Equation 16 gives information on the threshold for and the termination of impact damage in the coating.

3. Numerical analysis

Table I lists the input parameters used in the present study. Fig. 3 illustrates the effects of E_c and E_s on the flexure of the coating, $W(r)$. The maximum value of $W(r)$ occurs immediately beneath the point of impact and decreases with the increase in E_c and E_s. $W(r)$ monotonically decreases with the distance from the point of impact.

Fig. 4 illustrates the distribution of strain energy density in the coating, $\mathrm{d}U/\mathrm{d}r$, as a function of E_s for $E_c = 100$ GPa and coating thickness t_c for $E_s = E_s = 100$ GPa. To emphasize the behaviour in the region near to the point of impact, this distribution is shown only from $r = 0$ mm to $r = 0.2$ mm (as in Fig. 3 also). Each curve exhibits a maximum. With increase in E_c/E_s and t_c, the maximum value decreases and the radius at which it occurs shifts further from the point

TABLE I Input parameters[a] required for the numerical analysis in the present study

Kinetic energy of impactor[b]	$1/2MV^2 = 0.0001$ J
Coating thickness	$t_c = 150\,\mu$m
Elastic modulus of coating	$E_c = 25$, 100, or 400 GPa
Elastic modulus of substrate	$E_s = 25$, 100, 200, or 400 GPa
Poisson's ratio	$v_c = v_s = 0.25$

[a] The parameters are used in the numerical analysis, unless otherwise indicated.

[b] The change in the magnitude of the kinetic energy of impactor only shifts downward (or upward) the curves in Figs 3, 4, and 5, without changing the essential characteristics of the curves.

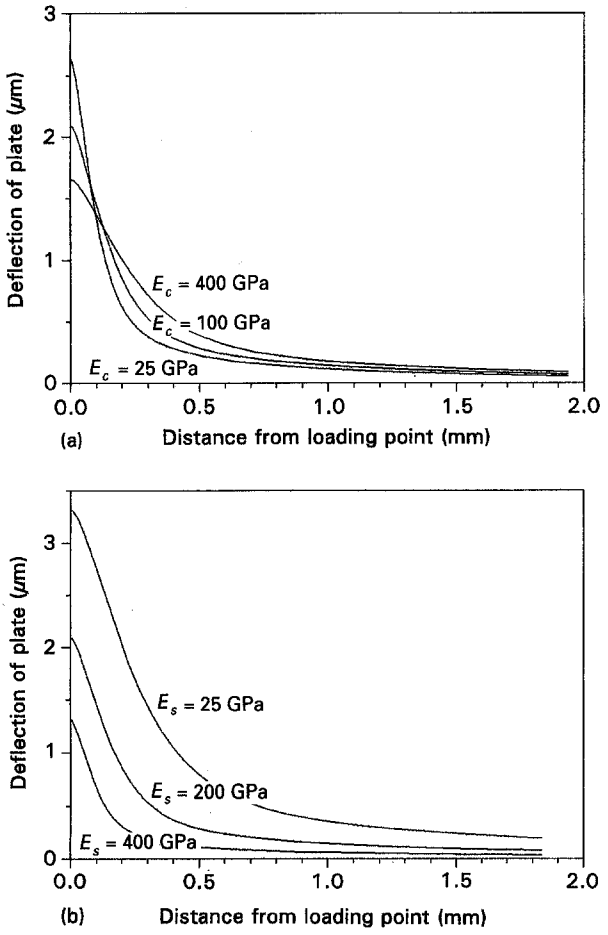

Figure 3 Impact-induced flexure of coating, as a function of (a) coating's elastic modulus $E_c(E_s = 100$ GPa) and (b) substrate's elastic modulus $E_s(E_c = 100$ GPa).

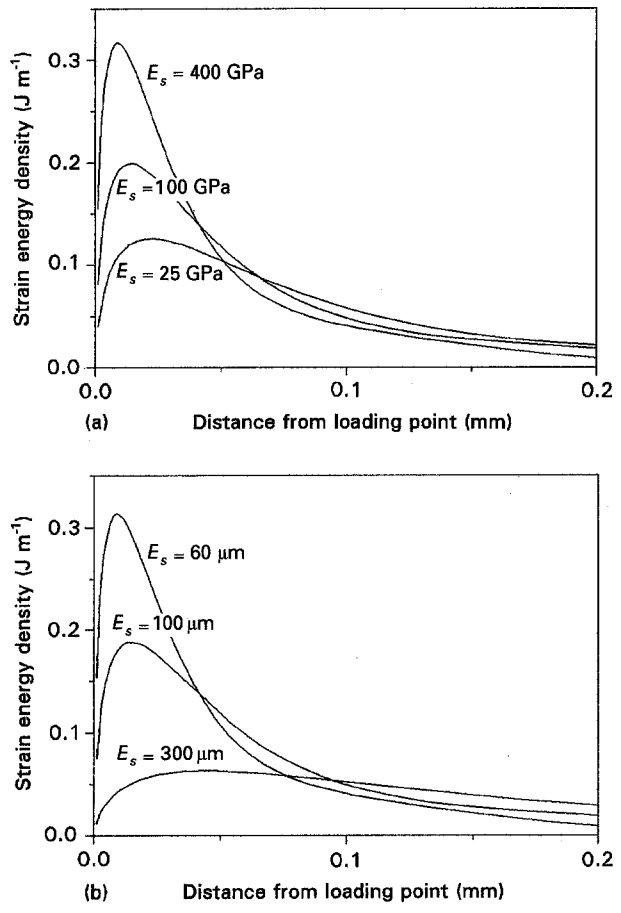

Figure 4 Influence of the change in (a) $E_s(E_c = 100$ GPa) and (b) t_c ($E_s = E_c = 100$ GPa) on the strain energy density distribution of coating, dU/dr.

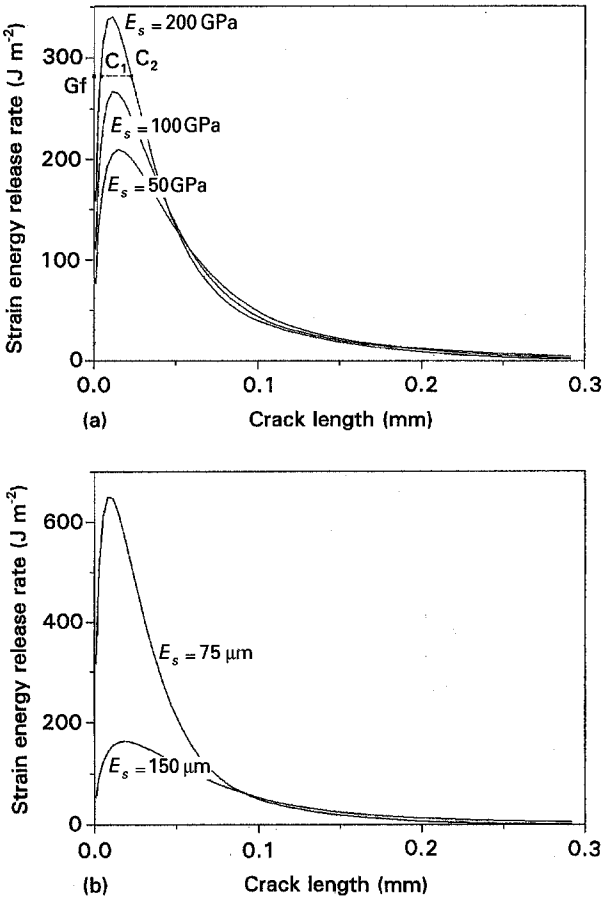

Figure 5 Strain energy release rate of coating, as a function of (a) $E_s(E_c = 100$ GPa) and (b) t_c ($E_c = 400$ GPa and $E_s = 100$ GPa)

of impact. The strain energy stored in the coating is calculated by integrating the area under the curve. Thus, it is clear that increases in E_c/E_s and t_c decrease the accumulation of strain energy in the neighbourhood of the point of impact. For instance, the total strain energy in the circular region of r 50.1 mm decrease with increasing E_c/E_s and t_c. If a local maximum strain energy density criterion of failure is adopted [20], increases in E_c/E_s and/or t_c can increase the resistance of coating to initiation of impact damage.

Fig. 5 is a plot of strain energy release rate G versus crack length C, showing that the maximum value of G decreases with the increase in E_c/E_s and/or t_c. Griffith's failure criterion indicates that crack propagation occurs if $G(C) > 2\tau$. For a given coating material, the length of the pre-existing crack $C = C_i$ immediately beneath the impact point is difficult to determine experimentally so that C_i remains an unknown variable. If $E_s = 200$ GPa and $2\tau = G_f$ (see Fig. 5a), the pre-existing cracks of length $C_1 < C_i < C_2$ can propagate. However, if $E_s = 50$ GPa and $2\tau = G_f$, no crack propagation occurs. Thus, the lateral crack model embodied in Equation 16 predicts that increases in E_c/E_s and/or t_c tend to decrease the probability of failure of the coating.

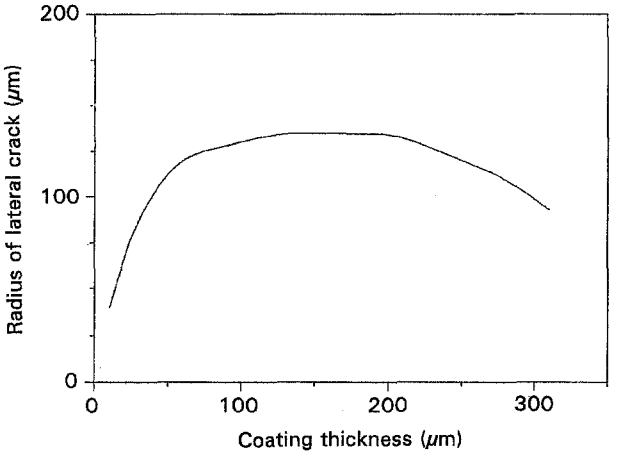

Figure 6 A plot of lateral crack radius C_2 versus coating thickness. $E_c = 400$ GPa and $E_s = 100$ GPa

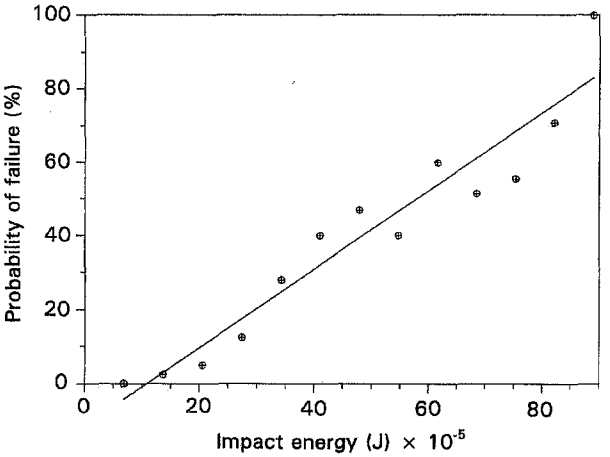

Figure 7 Probability of the impact induced failure of the glass slides resting on graphite substrate, with respect to impact energy.

The model thus accounts for the fact that stiff coatings are usually used to protect against erosive wear.

According to Griffith's failure criterion, crack arrest occurs if $G(C) < 2\tau$. To analyse the effect of coating thickness on the size C_2 of lateral crack developed, $\tau = 15\,\mathrm{J\,m^{-2}}$, $C_i = 13\,\mu\mathrm{m}$, and $t_c \geqslant 13\,\mu\mathrm{m}$ are substituted into Equation 16. Fig. 6 shows that the radius C_2 of the fully developed lateral crack is a nonlinear function of t_c. With an increase from $t_c = 13\,\mu\mathrm{m}$ to $t_c \approx 150\,\mu\mathrm{m}$, the radius C_2 increases and reaches a maximum. For $t_c > 150\,\mu\mathrm{m}$, C_2 decreases. Finally, the impact damage does not occur in coating layer when $t_c \geqslant 320\,\mu\mathrm{m}$. Generally speaking, radial cracks, cone cracks, and/or interface cracks may occur immediately after the impact damage (lateral crack) initiates. All such cracks can contribute to the release of the strain energy in a coating. Thus, the numerical result of Fig. 6, which is deduced from a model of a single and isolated lateral crack is only a qualitative prediction. For completeness, experimental work was performed on SiC-coated graphite specimens and model layered specimens.

4. Experimental procedure

Impact damage testing was performed on SiC-coated graphite and model layered specimens. The latter were prepared by resting commercial glass microscope slides on graphite substrates, glass plates, alumina substrates, and SiC whisker/Al_2O_3 composite tiles. The smooth interface between the glass slide and the substrate was wetted with water to promote adhesion by capillary action. The dimension of the glass slide was 17 mm × 17 mm × 0.146 mm. The thickness of substrate was > 3 mm. During testing, the layered specimen was set on a lead brick. Then a steel sphere with a weight of 0.699 g and a diameter of 5.55 mm was dropped vertically on to the layered specimens. Since the glass slide was transparent, the onset of impact-induced damage was examined by eye in transmitted light.

The SiC coated graphite specimens were prepared by chemical vapour deposition [21] (Material Technology Corp., Dallas, TX, USA). Using a diamond saw, the as-received billets were cut into specimens 8 cm × 0.8 cm × 0.5 cm, with the coating on one 8 cm × 0.8 cm surface. The coating was polished down to the desired thickness using diamond paste and its thickness was measured by viewing a cross-section under an optical microscope. An impactor with a weight of 21.7 g and a hemispherically-shaped head of radius 0.75 mm was dropped vertically onto the specimens. The impact-induced lateral cracks caused interference fringes in reflected light. Thus, the radius of the fringe could be measured using an optical microscope with a suitable filter. The occurrence of impact damage was determined by whether or not the fringe could be clearly observed by optical microscopy.

5. Results and discussion

Fig. 7 illustrates the relationship between impact energy and the probability of failure of glass slides resting on graphite substrates. The probability of failure is calculated by

$$\text{failure probability} = \frac{\text{number of impacts causing cracks}}{\text{total number of impacts}}$$

Each data point corresponds to 30 impacts. The linear regression line was calculated using the method of least squares. In this paper, the impact energy corresponding to 50% probability of failure is considered to be the critical energy required to initiate impact damage. Thus, the critical impact energy for glass slides resting on graphite substrates is about 5.8×10^{-4} J. Table II lists the elastic moduli of the various substrate materials, and Fig. 8 indicates the effect of modulus on the resistance of glass slides to initiation of impact damage. When the slides rest on a substrate with a smaller elastic modulus, more energy is needed to initiate impact damage. Increase in E_c/E_s apparently increases the resistance to impact damage, in agreement with the theoretical prediction.

Fig. 9a is an optical micrograph of impact damage on a SiC-coated graphite specimen. The number and length of the cracks on the surface of the coating do

TABLE II Elastic moduli of substrates and glass slides (units, GPA) [measured using a standing-wave technique [21]]

	Graphite substrate	Glass plate	Alumina substrate	SiC/Al_2O_3 composite	SiC coating layer	Glass slide
Elastic Modulus	10	68	306	403	376	68

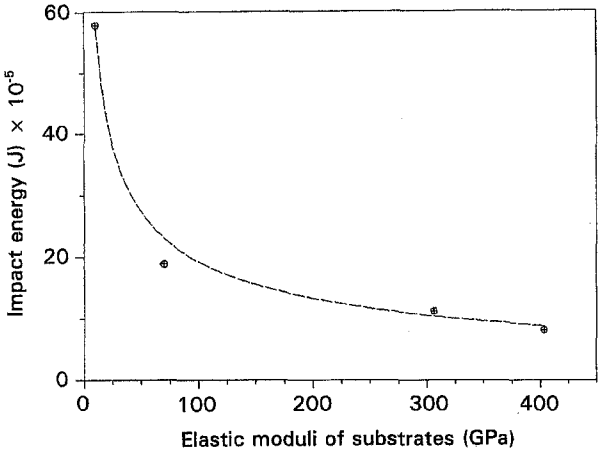

Figure 8 Effect of the change in substrate's elastic modulus on the critical energy required to initiate impact damage in glass slides.

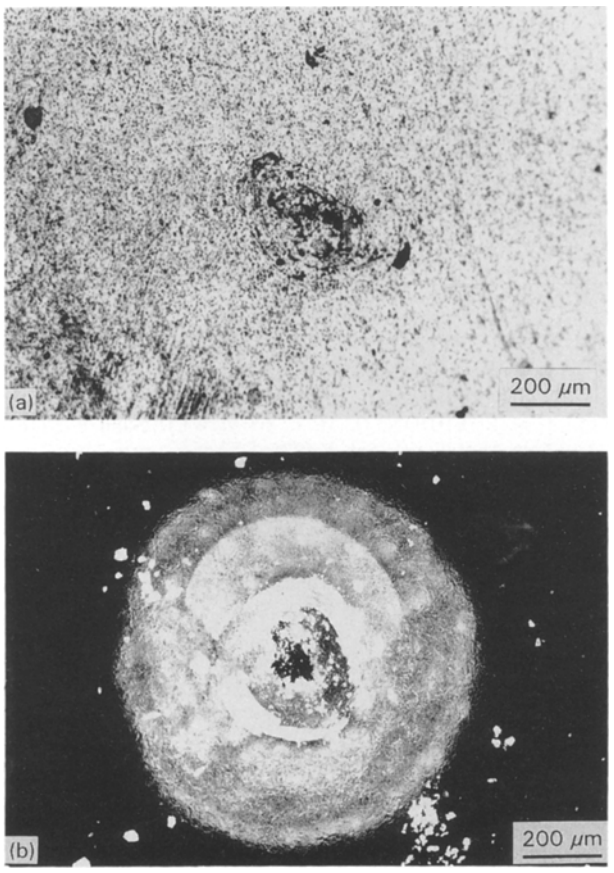

Figure 9 (a) An optical micrograph of an impact impression on SiC coating. (b) Interference fringe caused by the lateral cracks in the SiC coating layer.

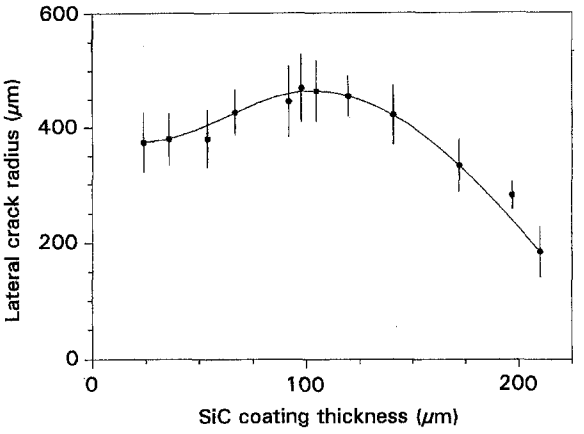

Figure 10 Variation of lateral crack radius with SiC coating thickness. Each data point represents at least six impact tests.

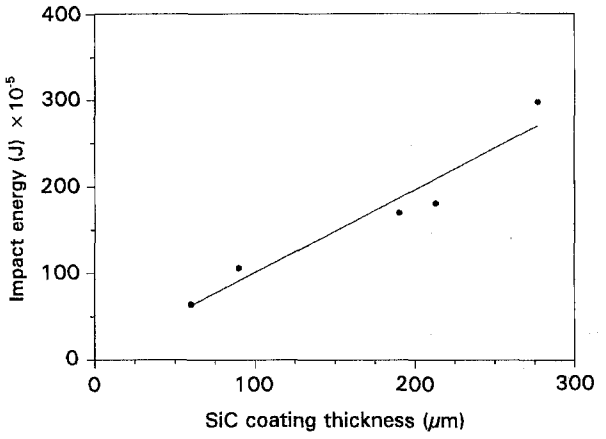

Figure 11 Relationship between the coating thickness and the critical energy required to initiate impact damage in SiC coating.

not exhibit any regular variation with impact loading or coating thickness. In contrast, the interference fringes caused by lateral cracks, which can be observed in reflected light using an optical microscope (see Figs 2b and 9b), shows a systematic variation of radius with the thickness of the coating. For example, the radius of fringe produced at an impact energy of 1.7×10^{-3} J initially increases with increasing coating thickness (Fig. 10). As the thickness of the coating increases further, the crack radius reaches a maximum. Finally, the interference fringes formed when $t_c \geqslant 210\,\mu m$ cannot be seen clearly by optical microscopy. The relationship between the radius of the lateral crack and the thickness of the coating exhibits a broad maximum, which agrees qualitatively with the theoretical prediction given in Fig. 6.

In the present study, the thickness of the SiC coating ranged from 24 μm to 277 μm. Fig. 11 indicates the

effect of this thickness on the impact energy required to initiate impact damage. It is seen that the resistance of the coating to initiation of damage increases with increasing thickness. The results agree with the theoretical prediction. However, the present authors believe that a coating of sufficient thickness, for instance $t_c \gg 277\,\mu m$, effectively "insulates" a given low-velocity impactor from the substrate. The impactor can not feel the existence of the substrate and the initiation of impact damage is determined only by the properties of the impactor and the SiC coating. Thus, the critical impact energy required to initiate impact damage may converge to a limiting value. As a result, the linear relationship between coating thickness and critical impact energy seen in Fig. 11 may occur only for "thin" coatings, and may not hold for a "thick" coating.

Strictly speaking, the theoretical analysis in the present paper is based on a simple low-velocity impact model. Even if the SiC coated graphite specimens reveal agreement between the experimental results and the theoretical analysis, studies of differently coated systems are still needed to understand impact damage in coatings.

6. Summary

The threshold for and development of low-velocity impact damage in coated materials has been studied in the present paper. Numerical analysis of a model of the growth of lateral crack has given the following results. (1) Increases in E_c/E_s and/or t_c have a tendency to increase the resistance of the coating to initiation of impact damage. (2) At constant impact energy, the size of the lateral crack is a function of coating thickness. Experimental results obtained from glass slides resting on various substrates show that such slides exhibit increasing resistance to impact damage as the elastic modulus of the substrate decreases. At an impact energy of 1.7×10^{-3} J, the radius of the impact-induced lateral crack in SiC-coating on graphite specimens varies with the thickness of the coating. An increase in SiC coating thickness from 24 μm to 277 μm improves the resistance of the coating to the initiation of impact damage.

Acknowledgement

The authors thank Michael B. Miller, Material Technology Corporation, Dallas, Texas, USA, for providing the SiC coating/graphite substrate composites.

Appendix A

The Bessel's integral for $J_n(x)$ is given by [22]

$$J_n(x) = \frac{1}{\pi}\int_0^{\pi} cos(n\theta - x\sin\theta)\,d\theta \qquad (A1)$$

where n is any positive integer. In the present study, the Bessel's integrals were carried out using the IMSL (International Mathematics and Statistics Library) subroutines.

Appendix B

Equation (12) is an empirical description of the distance from the free surface to the lateral crack. It can be replaced by other mathematical expressions which satisfy the initial condition $h(0) = 0$. For instance

$$h(r) = \frac{t_c}{A}\left[1 - \exp\left(\frac{-Br}{t_c}\right)\right] \qquad A \geq 1,\ B > 0 (B1)$$

and

$$h(r) = \frac{t_c}{A}\left[1 - \frac{1}{Br/t_c + 1}\right] \qquad A \geq 1,\ B > 0\ (B2)$$

are acceptable in the present study. Such a change in the form of the empirical equation does not change the essential characteristics of the curves shown in Fig. 5.

References

1. P. J. BURNETT and D. S. RICKERBY, *J. Mater. Sci.* **23** (1988) 2429.
2. G. ZAMBELLI and A. V. LEVY, Wear **68** (1981) 305–331.
3. C. C. CHIU, *J. Mater. Sci.* **27** (1992) 3353.
4. D. B. LEISER, R. CHURCHWARD, V. KATVALA, D. STEWART and A. BALTER, *Ceram. Eng. Sci. Proc.* **9** [9–10] (1988) 1125.
5. H. P. KIRCHNER and J. SERETSKY, *Am. Ceram. Soc. Bull.* **54** [6] (1975).
6. D. J. GREEN, *J. Am. Ceram. Soc.* **67** [8] (1986) 560.
7. B. M. LIAW, A. S. KOBAYASHI, A. F. EMERY and J. J. DU, "An Impact Damage Model of Ceramic Coatings", in "Fracture Mechanics of Ceramics", Vol. 7 (Plenum Press, New York, 1986, pp. 187.
8. W. T. CHEN, *Int. J. Engng. Sci.* **9** [9-A] (1971) 775.
9. W. T. CHEN and P. A. ENGEL, *Int. J. Solid Structures* **8** [11] (1972) 1257.
10. P. K. GUPTA and J. A. WALOWIT, *Trans. ASME, J. Lub. Tech.* **96** [4] (1974) 250.
11. R. B. KING and T. C. O'SULLIVAN, *Int. J. Solid Structures* **23** [5] (1987) 581.
12. G. S. SPRINGER, "Erosion by Liquid Impact" (John Wiley & Sons, New York, 1976) pp. 79–123.
13. A. P. S. SELVADURAI, "Elastic Analysis of Soil-Foundation Interaction (Elsevier Scientific Publishing Company, New York, 1979) p. 165.
14. I. N. SNEDDON, G. M. L. GLADWELL, and S. COEN, Lett. Appl. Engng. Sci. **3** (1975) 1.
15. H. L. CHEN, W. LIN, L. M. KEER and S. P. SHAH, *J. Appl. Mech.* **55** [12] (1988) 887.
16. K. N. SHIVAKUMAR, *J. Appl. Mech.* **52**[9] (1985) 675.
17. D. McFARLAND, B. L. SMITH and W. D. BERNHART, "Analysis of Plates" (Spartan Books, New York, 1972) p. 157.
18. S. SRINIVASAN and R. O. SCATTERGOOD, Wear **142** (1991) 115.
19. B. R. LAWN and M. V. SWAIN, *J. Mater. Sci.* **10** (1975) 113.
20. A. P. BORESI and O. M. SIDEBOTTOM, "Advanced Mechanics of Materials" (John Wiley & Sons, New York, 1985) p. 114.
21. C. C. CHIU and E. D. CASE, *Mater. Sci. Eng.* **A132** (1991) 39.
22. F. BOWMAN, "Introduction to Bessel Functions" (Longmans Green and Co., New York, 1938) p. 90.